Supporting Information for "Dual-tracer constraints on the Inverse-Gaussian Transit-time distribution improve the estimation of watermass ages and their temporal trends in the tropical thermocline"

Haichao Guo[1], Wolfgang Koeve[1], Andreas Oschlies[1,2], Yan-Chun He[3], Tronje Peer Kemena[1], Lennart Gerke[1], and Iris Kriest[1]

[1]GEOMAR Helmholtz Centre for Ocean Research Kiel, 24148, Kiel, Germany
[2]Kiel University, Kiel, Germany
[3]Nansen Environmental and Remote Sensing Center, Bjerknes Centre for Climate Research, Bergen, Norway

Correspondence: Haichao Guo (hguo@geomar.de)

Contents of this file

Text S1

We have calculated the CFC-12 and SF6 surface saturation for 25.45 $\mathrm{kg \cdot m^{-3}}$ to 25.55 $\mathrm{kg \cdot m^{-3}}$ at the outcrops in the Atlantic Ocean, Pacific Ocean, Indian Ocean, Arctic Ocean, and Southern Ocean. The hemispheric winter saturation state of CFC-12 generally increases from 1936 to 2015 in our FOCI *esm-piControl* simulations, i.e. without climate change (Fig. S3). This increasing trend might be caused by the changes of the increasing rate of atmospheric CFC-12 partial pressure (Shao et al., 2013; Raimondi et al., 2021). At different regions, the saturation state also differs, which might be due to the varying convection, magnitude of seasonality on CFC-12 solubility (potential temperature and salinity), air-sea gas exchange velocity, etc. Generally, the saturation state in the Atlantic and Pacific (from 90% to 100%) is higher than it in the North Indian Ocean (from 80% to 98%).

In the TTD calculation, the hemisphere from which the water originates might also matter, especially when considering slight differences in the tropospheric surface mixing ratio of CFC-12 and the saturation at isopycnal surfaces between the Northern and Southern hemispheres. In our calculation, we assume that no water moves across the equator and between ocean basins (except that waters from the Southern Ocean can move to the South Pacific Ocean, South Atlantic Ocean, and South Indian Ocean), i.e. waters in the Northern Hemisphere only originate from outcrops in the Northern Hemisphere. Also, the un-even saturation state of CFC-12 over outcrops, indicated by the standard deviation (Fig. S3), raises uncertainties of Γ considering the CFC-12 saturation state of water parcels. Therefore we calculate Γ considering the temporal change of the up-limit (mean

plus one standard deviation) and low-limit (mean minus one standard deviation) of the CFC-12 saturation state. For TTD calculation, we use the saturation-corrected CFC-12/SF6 mixing ratio history to constrain Δ/Γ.

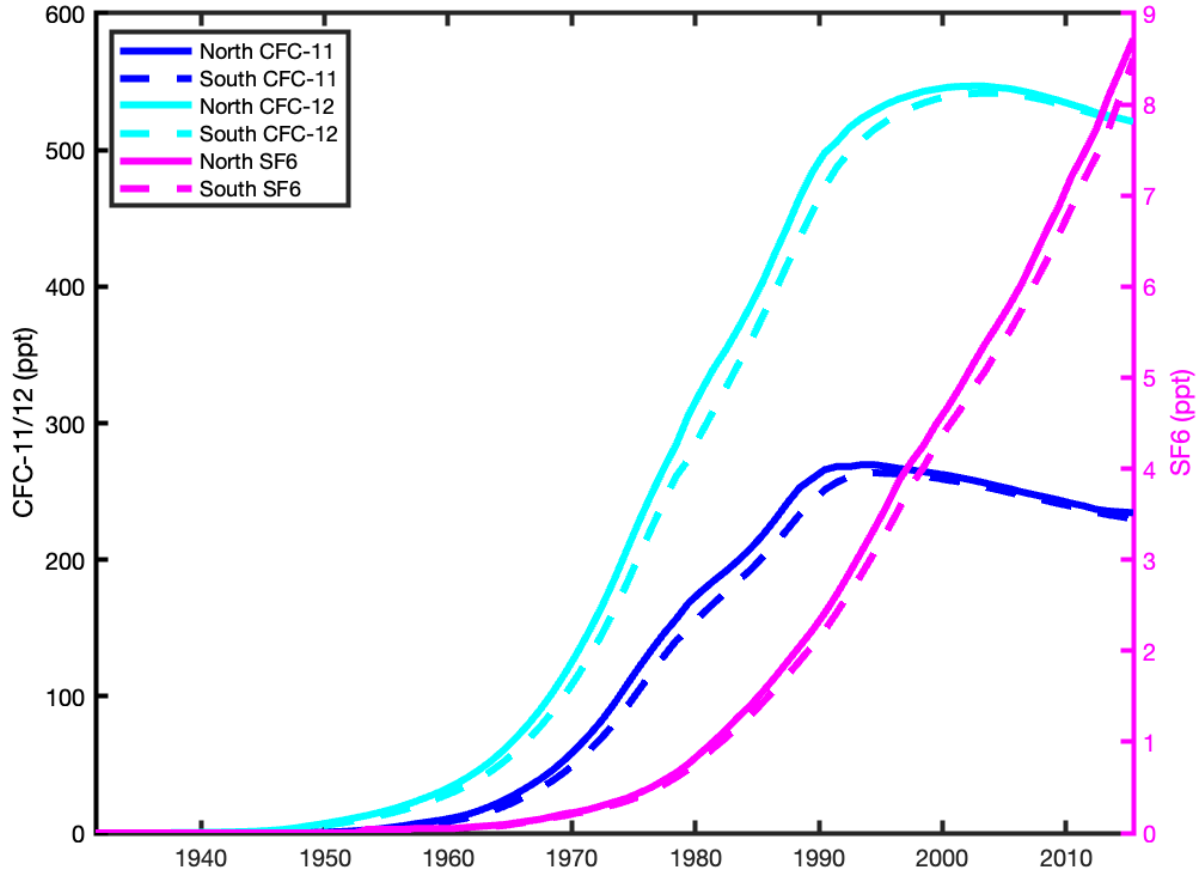

Figure S1. Observed histories of the annual mean atmospheric mixing ratio of CFC-11 (blue), CFC-12 (light-blue), and SF6 (purple) for the North Hemisphere (solid) and South Hemisphere (dash), with the unit of part per trillion (ppt) (Bullister, 2015).

References

Bullister, J. L.: Atmospheric Histories (1765-2015) for CFC-11, CFC-12, CFC-113, CCl_4, SF_6 and N_2O, Carbon Dioxide Information Analysis Center, Oak Ridge National Laboratory, US Department of Energy, Oak Ridge, Tennessee, https://doi.org/10.3334/CDIAC/otg.CFC_ATM_Hist_2015, 2015.

Raimondi, L., Tanhua, T., Azetsu-Scott, K., Yashayaev, I., and Wallace, D. W.: A 30-Year Time Series of Transient Tracer-Based Estimates of Anthropogenic Carbon in the Central Labrador Sea, Journal of Geophysical Research: Oceans, 126, e2020JC017 092, https://doi.org/10.1029/2020JC017092, 2021.

Shao, A. E., Mecking, S., Thompson, L., and Sonnerup, R. E.: Mixed layer saturations of CFC-11, CFC-12, and SF_6 in a global isopycnal model, Journal of Geophysical Research: Oceans, 118, 4978–4988, https://doi.org/10.1002/jgrc.20370, 2013.

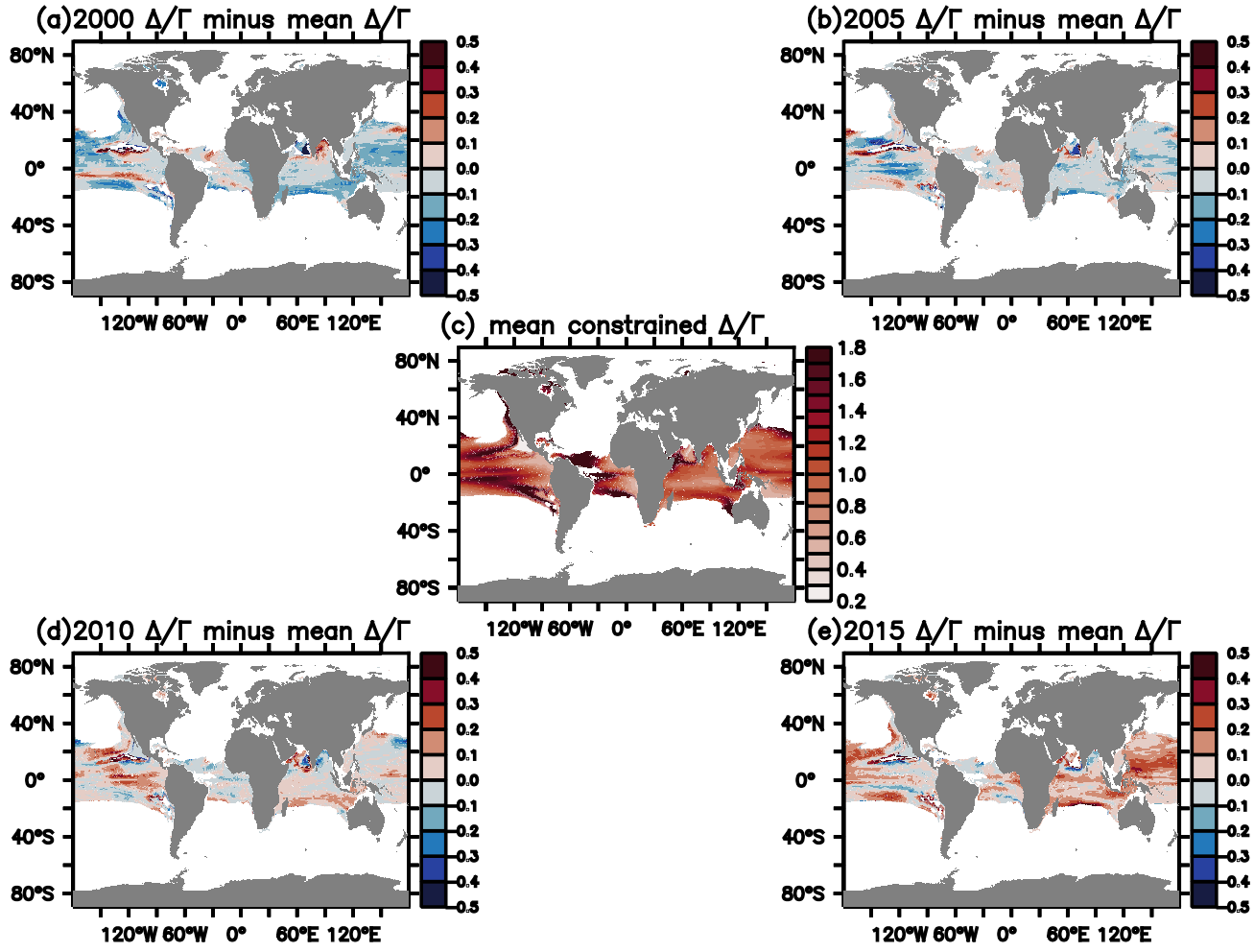

Figure S2. The same as Fig. 5, but for the *esm-hist* simulations.

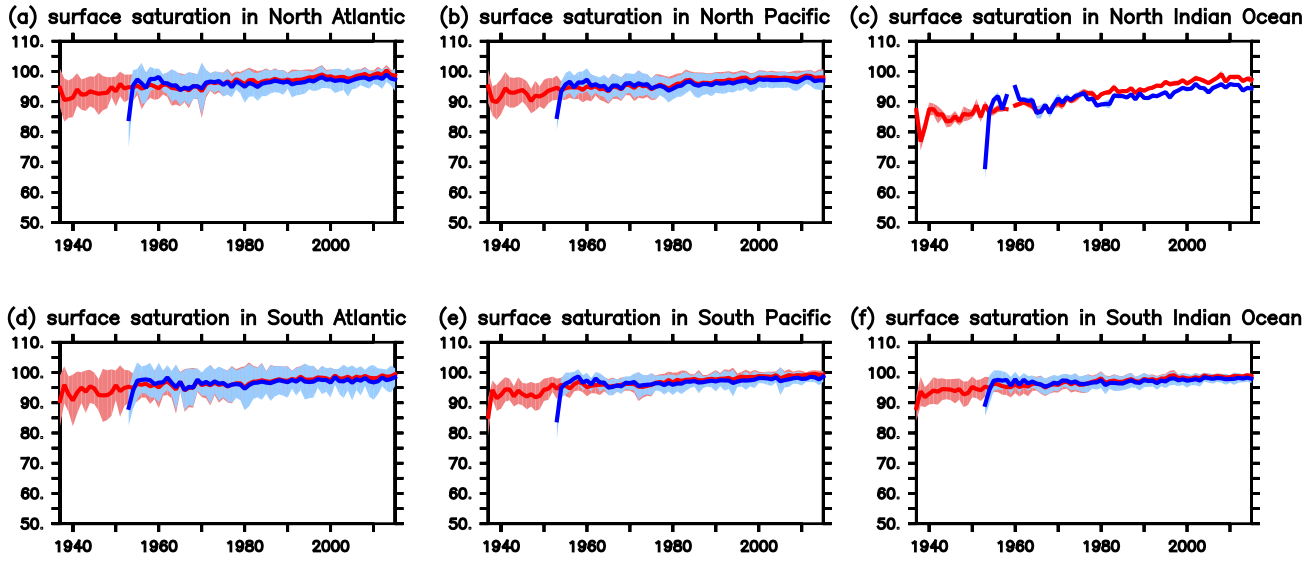

Figure S3. The temporal trend of the hemispheric winter saturation (in unit of %) of CFC-12 (red) and SF6 (blue) at outcrop of 25.5 $\mathrm{kg \cdot m^{-3}}$ in the *esm-piControl* simulation. The outcrop is calculated from March (northern hemisphere) and September (southern hemisphere) mean temperature and salinity. The shading color is the surface saturation's standard deviation at the outcrop.

Table S1. Mean state and temporal trends of ideal age and mean age of the IG-TTD applying spatial homogeneous and CFC-12 and SF_6 constrained Δ/Γ in *esm-piControl* simulations from 1981 to 2015. We focus on the upper tropical thermocline (σ_0=25.5 $\mathrm{kg \cdot m^{-3}}$). "$\pm$" means 95% confidence interval.

Variable	Mean state (yr)	Trends (yr/yr)
ideal age	46.0 $\pm$ 0.8	-0.016 $\pm$ 0.012
mean age (Δ/Γ=0.8)	22.0$\pm$ 2.0	0.091$\pm$ 0.016
mean age (Δ/Γ=1.0)	25.6$\pm$ 1.1	-0.036 $\pm$ 0.014
mean age (Δ/Γ=1.2)	29.8$\pm$ 3.7	-0.178 $\pm$ 0.015
mean age (Δ/Γ=1.4)	35.1$\pm$ 6.9	-0.340 $\pm$ 0.018
mean age (constrained Δ/Γ:2000)	26.0$\pm$ 0.9	-0.018 $\pm$ 0.015
mean age (constrained Δ/Γ:2005)	26.0$\pm$ 1.0	-0.026 $\pm$ 0.014
mean age (constrained Δ/Γ:2010)	25.9$\pm$ 1.2	-0.039 $\pm$ 0.015
mean age (constrained Δ/Γ:2015)	25.6$\pm$ 1.3	-0.043 $\pm$ 0.016

Table S2. The same as Table S1, but for the *esm-hist* simulation.

Variable	Mean state (yr)	Trends (yr/yr)
ideal age	47.9 $\pm$ 1.6	0.056 $\pm$ 0.019
mean age (Δ/Γ=0.8)	23.8$\pm$ 2.6	0.115$\pm$ 0.020
mean age (Δ/Γ=1.0)	27.8$\pm$ 1.2	-0.009 $\pm$ 0.020
mean age (Δ/Γ=1.2)	32.9$\pm$ 3.3	-0.151 $\pm$ 0.022
mean age (Δ/Γ=1.4)	39.0$\pm$ 6.5	-0.313 $\pm$ 0.026
mean age (constrained Δ/Γ:2000)	26.6$\pm$ 1.7	0.064 $\pm$ 0.019
mean age (constrained Δ/Γ:2005)	26.1$\pm$ 1.6	0.055 $\pm$ 0.020
mean age (constrained Δ/Γ:2010)	27.5$\pm$ 1.3	0.017 $\pm$ 0.021
mean age (constrained Δ/Γ:2015)	28.3$\pm$ 1.3	-0.016 $\pm$ 0.021